Conformation of Human Apolipoprotein C-I in a Lipid-Mimetic Environment Determined by CD and NMR Spectroscopy[†,‡]

Annett Rozek,[§,||] James T. Sparrow,[⊥] Karl H. Weisgraber,[#] and Robert J. Cushley*[,§]

Department of Chemistry and Institute of Molecular Biology and Biochemistry, Simon Fraser University, Burnaby, British Columbia V5A 1S6, Canada, Baylor College of Medicine, The Methodist Hospital, Houston, Texas 77030, Department of Pathology, Gladstone Institute of Cardiovascular Disease, Cardiovascular Research Institute, University of California, San Francisco, California 94140-0608

Received December 17, 1998; Revised Manuscript Received August 11, 1999

ABSTRACT: The high-resolution conformation of human apoC-I in complexes with sodium dodecyl sulfate (SDS) is presented. As estimated from CD data, apoC-I adopts 54% helical secondary structure when bound to SDS, which is similar to the helical content previously found with phospholipids. The NMR-derived conformation of apoC-I is composed of two amphipathic helices, residues 7−29 and 38−52, separated by a flexible linker. The N-terminal helix contains a mobile hinge involving residues 12−15. The hydrophobic side chains cluster on the nonpolar face of both helices, thus forming two discrete lipid-binding sites in the N-terminal helix and one in the C-terminal helix. As suggested by amide proton resonance line widths and deuterium exchange rates, the N-terminal helix is more flexible and may bind less tightly to the detergent than the C-terminal helix. The different mobility of both helices appears to be related to side-chain composition, rather than length of the amphipathic helix, and may play a role in the function of apoC-I as an activator of lecithin:cholesterol acyltransferase (LCAT). A model is suggested in which the C-terminal helix serves as a lipid anchor while the N-terminal helix may hinge off the lipid surface to make specific contacts with LCAT.

Human apolipoprotein (apo)[1] C-I is a 57-residue exchangeable plasma apolipoprotein mainly distributed in high-density lipoprotein (HDL) and very low-density lipoprotein (VLDL). ApoC-I has been shown to fulfill various functions in vitro, such as modulation of enzymatic activity and lipoprotein binding to receptors. ApoC-I is a secondary activator of lecithin:cholesterol acyltransferase (LCAT) (*1*, *2*), an enzyme which is responsible for plasma cholesteryl ester formation (*3*); the primary activator of LCAT being apoA-I. ApoC-I was reported to inhibit phospholipase A_2 (*4*) and hepatic lipase (*5*) and to stimulate cell growth (*6*). One function, which appears to be highly specific to apoC-I, is the modulation of apoE content in VLDL and the inhibition of apoE-mediated binding of VLDL remnants to the low-density lipoprotein receptor-related protein (LRP) (*7*). ApoC-I also inhibits the apoE-dependent cellular metabolism of VLDL through the low-density lipoprotein receptor pathway (*8*). In line with these results, recent studies in vivo report that transgenic mice overexpressing human apoC-I show highly elevated serum cholesterol and triglyceride levels due to impaired clearance of VLDL remnants by the liver (*9*).

The apolipoprotein genes are similar in that they contain four exons and three introns. Exons 3 and 4 are the coding regions for the amino acid sequence, which is characterized by regular 11 or 22 codon repeats (*10*). As the smallest member of the apolipoprotein family, apoC-I is considered to be very similar to the primordial gene from which apolipoproteins have evolved via duplication and deletion of 11 codon repeats (*11*). The amino acid sequence of apoC-I (*12*, *13*) contains four 11mer repeats, three of which are encoded by exon 3 (residues 7−39) and one encoded by exon 4 (residues 40−50). The close linkage of the apoC-I and apoE genes on human chromosome 19 (*14*, *15*) has prompted studies on the possible relation of apoC-I to Alzheimer's disease. By screening Alzheimer's patients it was found that the presence of an apoC-I restriction site in disequilibrium with the apoE4 allele may be an additional risk factor (*16*).

The observation that the α-helical content of apolipoproteins increases upon binding to phospholipid has led Segrest and co-workers (*17*) to propose the amphipathic helix to be

[†] This work was supported by the Heart and Stroke Foundation of B.C. & Yukon and, in part, by a National Institutes of Health (NIH) Program Project Grant, HL 41633. The NMR facility was financed in part by the Natural Science and Engineering Research Council of Canada.

[‡] The coordinates and NMR restraints of apoC-I have been deposited in the Brookhaven Protein Data Bank, PDB filename 1IOJ.

* To whom correspondence should be addressed. Phone: (604) 291-4230. Fax: (604) 291-5583. E-mail: cushley@sfu.ca.

[§] Present address: Department of Microbiology and Immunology, University of British Columbia, Vancouver, British Columbia, V6T 1Z3, Canada.

[||] Department of Chemistry and Institute of Molecular Biology and Biochemistry.

[⊥] Baylor College of Medicine.

[#] Department of Pathology.

[1] Abbreviations: apo, apolipoprotein; HDL, high-density lipoprotein; VLDL, very low-density lipoprotein; LCAT, lecithin: cholesterol acyltransferase; CD, circular dichroism; SDS, sodium dodecyl sulfate; TOCSY, total correlated spectroscopy, DQF-COSY, double quantum filtered correlated spectroscopy, NOESY, nuclear Overhauser enhancement spectroscopy; NOE, nuclear Overhauser effect; HSQC, heteronuclear single quantum coherence; RMS, root-mean-square; DSSP, dictionary of secondary structure in proteins.

10.1021/bi982966h CCC: $18.00
Published on Web 10/12/1999

an essential structural motif in lipid−protein interaction. An amphipathic helix is defined as an α-helix with opposing polar and nonpolar faces oriented along the long axis of the helix. The nonpolar face is composed of hydrophobic amino acids and interacts with the fatty acyl chains of the lipid, while the polar face contains hydrophilic amino acids, which extend toward the lipid headgroups and the aqueous milieu. Thus, the amphipathic helix is embedded into the surface of the lipoprotein particle. ApoC-I is predicted to form two such helices extending over residues 7−32 and 33−54 (*18*).

The lipid-bound structure of apoC-I may serve as a model for apolipoprotein structure−function relationships in general. For example, understanding the mechanism of LCAT activation should be greatly aided by knowledge of the conformation of one of its activator proteins, e.g., apoC-I. In this communication, we describe the detailed structure of apoC-I in the presence of sodium dodecyl sulfate (SDS) micelles which are often used to model the environment of membrane-associating peptides and proteins (*19*, *20*). This is the first reported high-resolution structure of an intact human serum apolipoprotein in a lipid-mimetic environment. The apoC-I complexes with SDS are amenable to detailed structural analysis by solution NMR methods since they reorient faster than complexes with phospholipid. Previously, we have determined the structures of three apoC-I fragments bound to SDS under similar experimental conditions (*21*, *22*). The structural agreement of apoC-I with its fragments is discussed.

EXPERIMENTAL PROCEDURES

The CD spectra were recorded on a Jasco J710 spectropolarimeter calibrated using *d*-(+)-camphorsulfonate. To an aqueous solution of apoC-I (c = 0.07 mM) were added aliquots of an SDS stock solution up to a molar apoC-I:SDS ratio of 1:10. Spectra were the average of two scans from 190 to 260 nm, recorded with a band width of 0.5 nm and a scan rate of 5 nm/min. Following subtraction of the blank spectrum and baseline correction, the observed ellipticities were converted to mean residue molar ellipiticities $[\theta]$ (deg cm^2 dmol^{-1}). The secondary structure content was estimated by deconvoluting the spectra using convex constraint analysis (*23*) and from the $[\theta]_{222}$ value using the relation %helix=($|[\theta]|_{222}$ + 3000)/(36 000 + 3000) (*24*).

The NMR spectra of native human apoC-I, isolated from blood plasma, and selectively ^{15}N-labeled synthetic apoC-I were recorded on a Bruker AMX600 spectrometer at 50 °C and pH 4.8. The NMR samples of native apoC-I and synthetic ^{15}N-labeled apoC-I were 5.8 and 5 mM in protein, respectively, at a molar protein to SDS-d_{25} ratio of 1:40. Resonance assignments were obtained from two-dimensional TOCSY (*25*), DQF-COSY (*26*), and NOESY (*27*) spectra and from ^{15}N-filtered TOCSY and NOESY (*28*, *29*) spectra. In addition, ^{15}N-HSQC (*30*), TOCSY-HSQC, and NOESY-HSQC (*31*) were used to confirm assignments. Details on NMR data acquisition, NMR spectra, and amino acid assignments for apoC-I were reported previously (*32*). The NOE-based distance restraints were obtained from the NOESY spectra of both the native and the synthetic sample. The bulk of restraints was generated from the NOESY spectra collected with a mixing time of 75 ms. The NOE cross-peaks were integrated with the FELIX 95.0 program (Molecular Simulations Inc., San Diego, CA). The NOE volumes were classified into three overlapping distance ranges, strong (1.8−3.0 Å), medium (2.5−4.0 Å), and weak (3.5−5.0 Å). The NOEs observed in NOESY spectra with mixing times of 100 and 150 ms were classified as weak. Cross-peaks which were overlapped more than 50% were treated as weak restraints in distance geometry calculations and as a separate "overlapped" distance class in minimization and restrained molecular dynamics calculations. Pseudo-atom corrections were applied to methylene protons and methyl groups by adding 1 and 1.5 Å, respectively, to the upper bounds. An ensemble of 50 structures was generated with the distance geometry-simulated annealing program DGII (Molecular Simulations Inc., San Diego, CA) using 685 NOE-based distance restraints, (264 intraresidue, 336 interresidue, and 85 overlapped restraints), essentially as described (*21*). No dihedral angle restraints and no hydrogen bond restraints were used. All structures were subjected to extensive minimization, including a short molecular dynamics, using the Discover program (Molecular Simulations, Inc.) with the consistent valence force field (CVFF) (*33*). In minimization and dynamics calculations the NOE distance restraints were applied with square-well potentials and maximal force constants of 50 kcal/mol. Since it is difficult to accurately simulate the detergent micelle−water interface, we decided to minimize the impact of electrostatic interactions on the structures. The dielectric constant was set to 1 and formal charges were switched off. In this way the efficacy of NOE distance restraints was maximized. Minimization consisted of two phases: (i) 10 000 steps (or 0.01 maximum RMS derivative) using the steepest descend algorithm and (ii) 25 000 steps (or 0.001 maximum RMS derivative) using the conjugate gradient algorithm. The restrained molecular dynamics was run over 2 ps at 500 K and 1 ps at 300 K and was followed by another two-phase minimization. The minimization and molecular dynamics calculations effected an improved helical geometry and a lower total energy of the structures. The final structures were analyzed using the Insight 95.0 program (Molecular Simulations Inc., San Diego, CA), the MOLMOL program (ETH Zürich, Switzerland), and the WHAT IF/WHAT CHECK program (1997, G. Vriend and R. W. W. Hooft).

The resonance line widths of amide protons were measured from NOESY cross-peaks. The NOESY spectrum (τ_m = 150 ms, resolution in acquisition dimension 3.4 Hz) was processed to a 4K × 2K matrix. An F2 slice through the center of the NOESY cross-peak of a side-chain proton, usually H^α (F1), with the amide proton (F2) was fitted using the deconvolution routines available in the XWIN-NMR 1.2 program (Bruker, Karlsruhe, Germany), thus extracting the line width. The uncertainty in the line width determination is ±4 Hz as estimated from the variation among cross-peaks to different side-chain protons.

Approximate deuterium exchange rates were determined from the time necessary to exchange the amide proton against deuterium. The protein in SDS solution was lyophilized and redissolved in 99% D_2O (Cambridge Isotope Laboratories Inc, Andover, MA). A NOESY spectrum was acquired at 50 °C between 2 and 7 h after adding D_2O. The degree of amide proton exchange against deuterium was estimated from the intensity of the $H^N-H^{side\ chain}$ cross-peaks as follows: absent = fast, small = medium, strong = slow.

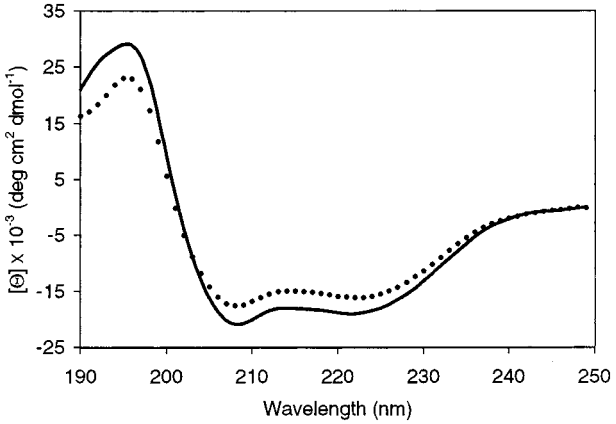

FIGURE 1: Circular dichroism spectra, recorded at 25 °C and pH 6, of apoC-I in the absence of SDS (dotted line) and in the presence of a 5-fold molar excess of SDS (solid line).

RESULTS

Circular Dichroism Spectroscopy. CD spectroscopy of apoC-I was carried out in order to estimate the amount of SDS needed for saturation and the maximum helicity of apoC-I. The CD spectra are shown in Figure 1. The CD curves have the signature of a helical structure with a maximum at 195 nm and two minima at 208 and 222 nm. The results of convex constraint analysis (*23*) of the CD spectra are presented in Table 1. In the absence of SDS, apoC-I contains about 42% helix. The deviation between our value and the one recently reported for the monomeric state of apoC-I (30%) (*34*) likely arises from oligomerization due to the higher apoC-I concentration used in our experiments (0.07 vs 0.001 mM) (*35*). Upon the addition of SDS, the helicity of apoC-I increases to a maximal value of 54% at a molar apoC-I:SDS ratio of 1:5. SDS−polyacrylamide gel electrophoresis of the solution at a molar apoC-I:SDS ratio of 1:10 indicated that apoC-I was in the monomeric state.

The maximum helicity of apoC-I bound to SDS, estimated from the $[\theta]_{222}$ value (−18 200 deg cm^2 dmol^{-1}) by the method of Greenfield and Fasman (*24*), is also 54%. The helical content of apoC-I in SDS is similar to the helical content of apoC-I in egg yolk phosphatidylcholine−cholesterol complexes (50%), which have a diameter of about 130 Å and represent the most physiological model of a lipoprotein particle (*2*). A good agreement also exists between the apoC-I helicity in SDS and DMPC (53%) (*36*).

Global Structure. The NMR spectra of native human apoC-I, isolated from blood plasma, and selectively ^{15}N-labeled synthetic apoC-I, were acquired in the presence of SDS at 50 °C and pH 4.8. Panels A and B of Figure 2 show the H^N-H^α and H^N-H^N regions, respectively, of the homonuclear NOESY spectrum, indicating amino acid assignments. Cross-peaks are well resolved in the C-terminal part of the protein, residues 40−53, due to aromatic ring current effects exerted by Trp41, Phe42, and Phe46. Complete proton resonance assignments were obtained using homonuclear and ^{15}N-filtered two-dimensional NMR spectroscopy and were published previously (*32*). A schematic summary of cross-peaks observed in the NOESY spectra and the chemical shift index (CSI) of α-protons is given in Figure 3. The CSI was

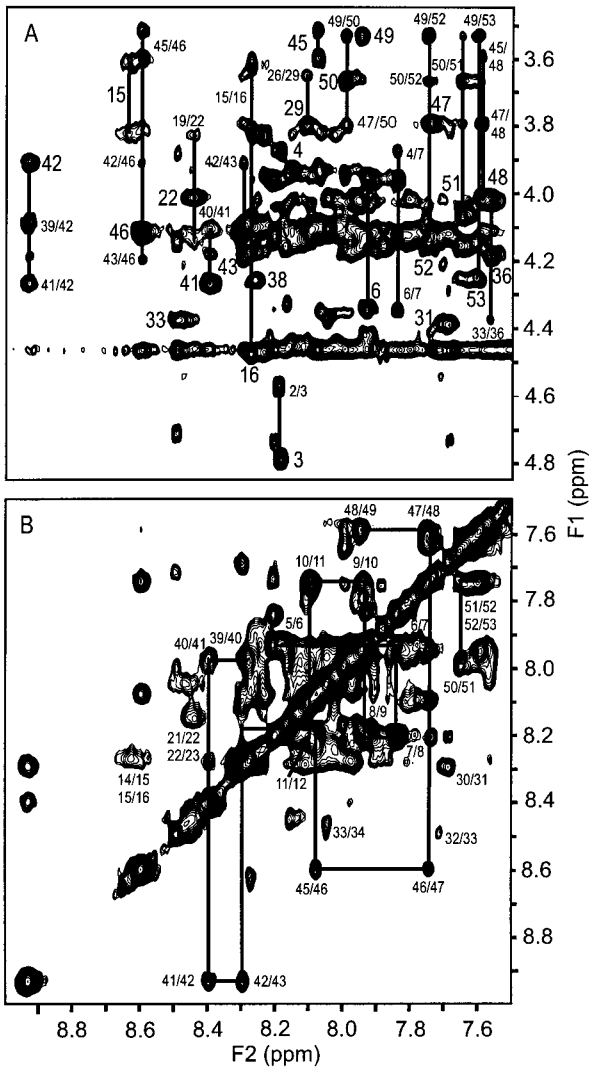

FIGURE 2: The H^N-H^α (A) and H^N-H^N (B) regions of the NOESY spectrum (mixing time 150 ms) of apoC-I, acquired at 600 MHz, 50 °C, pH 4.8, at a molar protein:SDS ratio of 1:40. Resolved intraresidue, sequential, and medium range cross-peaks are labeled with the residue number(s). Reproduced with permission from ref *32*.

Table 1: Percentage of Secondary Structure Types Estimated by CD Spectroscopy[a]

molar apoC-I to SDS ratio	secondary structure type (%)[b]					
	α-helix	β-turn	β-structure and unordered structure	unordered	unordered structure and additional chiral contribution	additional chiral contribution
no SDS	42	18		26		14
1:1	44	20		25		11
1:5	54		26		20	
1:10	55		25		21	

[a] The data were collected at 25 °C and pH 6. The experimental error in secondary structure content is about ±15%. [b] Percentage of secondary structure types was obtained by convex constraint analysis (*23*).

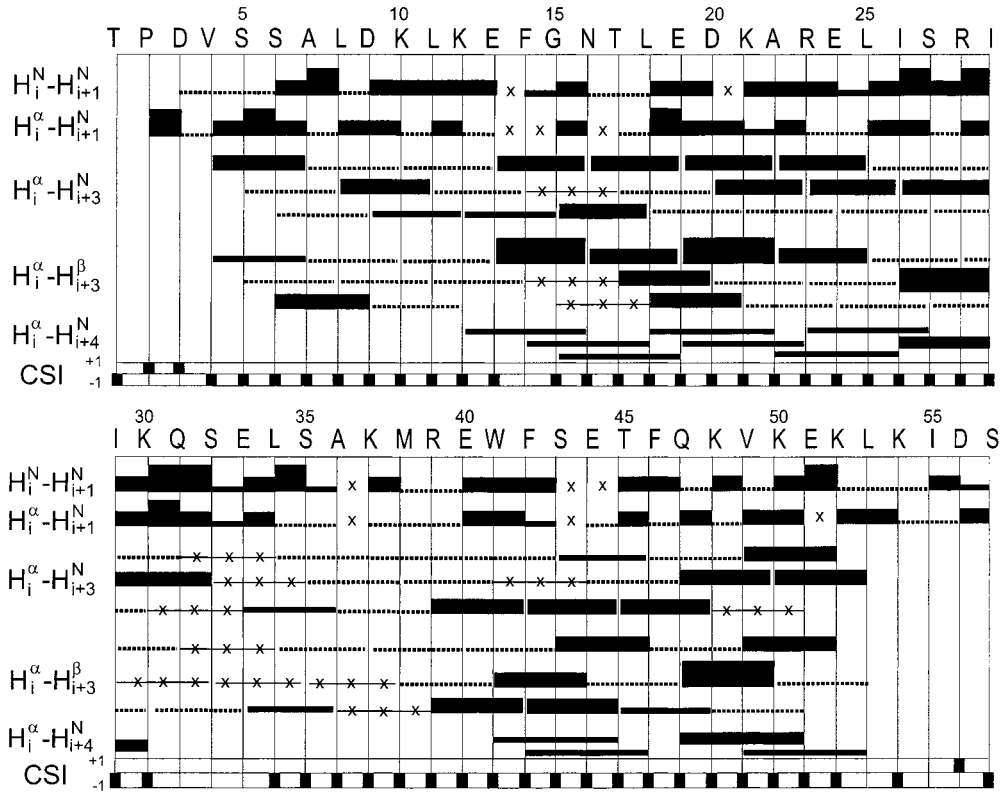

FIGURE 3: Interresidue NOE contacts observed in the NOESY spectra of apoC-I and chemical shift index (CSI) of α-protons. The intensity of the NOE connectivity is indicated by the thickness of the solid black bars. Dashed lines indicate potential NOE cross-peaks, which may be hidden or ambiguous due to resonance overlap. Crosses and lines with crosses indicate definitely absent NOE cross-peaks. The CSI of α-protons was calculated as described by Wishart et al. (*37*). Reproduced with permission from ref *32*.

determined from the difference between measured and random coil chemical shifts (*37*). The mostly negative CSI and the abundance of NOE contacts with a range of three and four residues indicate a helical structure for apoC-I as expected from the CD data. Detailed three-dimensional structures were calculated by distance geometry-simulated annealing and restrained molecular dynamics methods based on 685 NOE-derived distance restraints. Figure 4 shows the global fold of apoC-I. The protein forms two helices separated by a flexible linker, which allows the two helices to adopt a wide range of orientations relative to each other. The 50 calculated structures fall into two groups, a "closed" conformation with helix−helix distances shorter than 5 Å, and another "open" V-shaped conformation. Since we did not observe long-range NOEs which would point to closely associated helices, only the 18 "open" conformations, which also have small residual NOE restraint violations, are discussed in this report. The structural statistics of these 18 structures are summarized in Table 2.

Figure 5A shows the distribution of distance restraints per amino acid residue, while Figure 5B shows the local root-mean-square (RMS) deviation of the 18 apoC-I structures. Two well-defined regions, having RMS deviations below 0.5 Å, appear in the N-terminal and C-terminal half of apoC-I. Analysis of the backbone torsion angles, shown in Figure 5C, and of the hydrogen bond pattern with the DSSP program (*38*) indicates helical geometry for the regions 7−29 and 38−52. The average pairwise backbone (N−C^α−C′) RMS deviations are 2.43 ± 0.99 Å for residues 7−29 and 1.85 ± 0.93 Å for residues 38−52. These high RMS deviations for the whole helical regions, as opposed to low local RMS deviations, are due to bends in each helix. The convergence

Table 2: Statistics for the Calculated Structures of Human ApoC-I[a]

no. of NOE distance restraints	
total	685
intraresidue	264
interresidue	336
overlapped	85
no. of NOE distance restraint violations > 0.1 Å	2.7 ± 1.8
largest NOE distance restraint violation (Å)	0.14 ± 0.05
RMS deviations from ideal geometry	
bonds (Å)	0.025 ± 0.000
angles (deg)	2.625 ± 0.086
Energies (kcal mol^{-1})[c]	
E_{total}	719 ± 16
E_{bond}	141 ± 2
E_{angle}	273 ± 10
$E_{torsion}$	59 ± 7
$E_{out-of-plane}$	2 ± 0
E_{VdW}	146 + 14

Atomic RMS Deviations (Å)

residues	backbone (N−C^α−C′)	all heavy
7−11	0.78 ± 0.56	1.99 ± 0.87
12−29	0.97 ± 0.37	2.13 ± 0.34
38−46	0.66 ± 0.29	1.97 ± 0.49
47−52	0.40 ± 0.16	1.86 ± 0.40

[a] Eighteen of 50 calculated structures we analyzed. [b] Energies are specific to the CVFF force field as implemented in the Discover program (Molecular Simulations Inc, San Diego, CA).

of the 18 calculated apoC-I structures was also analyzed by calculating the order parameter for backbone torsion angles, which varies between the value 1 for exactly defined angles and the value 0 for random angles (*39*). The order parameters

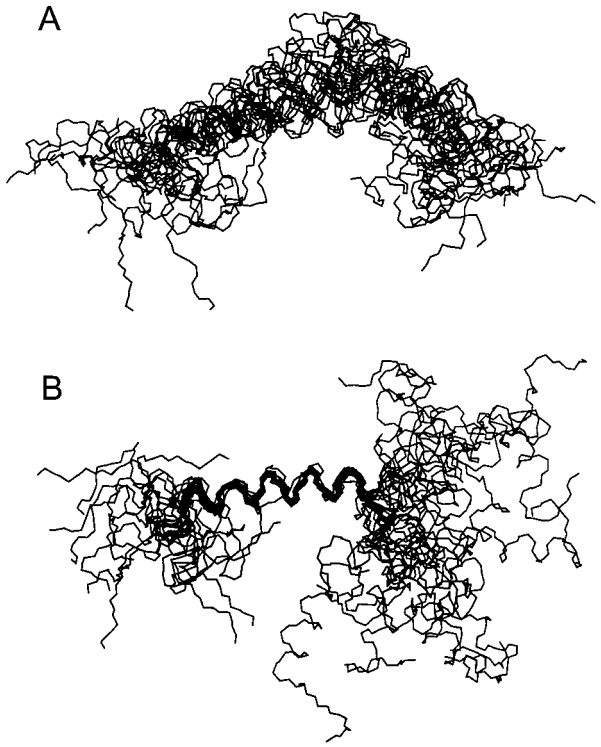

FIGURE 4: Global fold of 18 calculated structures of human apoC-I. The backbone atoms (N−C^{α}−C′) of all residues are shown. (A) Superposition of both helical regions, 7−29 and 38−52, showing the "V"-shape of each molecule. (B) Superposition of residues 12−29 of the N-terminal helix indicating the range of orientations of the two helices relative to each other.

for backbone torsion angles, plotted in Figure 5D, average to 0.89 ± 0.11 for the N-terminal helix and to 0.87 ± 0.19 for the C-terminal helix.

Figure 6A shows a ribbon representation of the structure closest to the mean of the 18 "open" conformations. The ribbon's width and color vary to reflect the circular variance of the dihedral angle ψ. Regions in deeper red and of larger width represent increased disorder relative to the well-defined yellow regions. Poorly defined regions are both the N- and C-terminus, the interhelical region between residues 30−37, and two helical bends centered at residues 11/12 in the N-terminal helix, and residues 46/47 in the C-terminal helix. Panels B and C of Figure 6 show the distribution of straight and bent conformations in the N-terminal and the C-terminal helix, respectively. Panels D and E of Figure 6 illustrate the orientation of the side chains in apoC-I in the N-terminal and the C-terminal helix, respectively, with one example each for the straight and bent conformations. Independent of the backbone orientation, both the N-terminal and the C-terminal helix are amphipathic and their side-chain arrangement is that of a class A helix, which is deemed to be ideal for phospholipid binding (*40*).

N-Terminal Lipid-Binding Domain. The N-terminal helix is formed by residues 7−29. The position of the first helical turn, residues 7−10, with respect to the remainder of the N-terminal helix fluctuates due to a bend at residues 11/12 (Figure 6B). The torsion angles of residues 11−15 vary considerably (Figures 5D and 6A), and the RMS deviations are higher (Figure 5B). The bend at 11/12 is a direct consequence of the absence of NOE distance restraints to the amide protons of residues 12−15 due to broad backbone

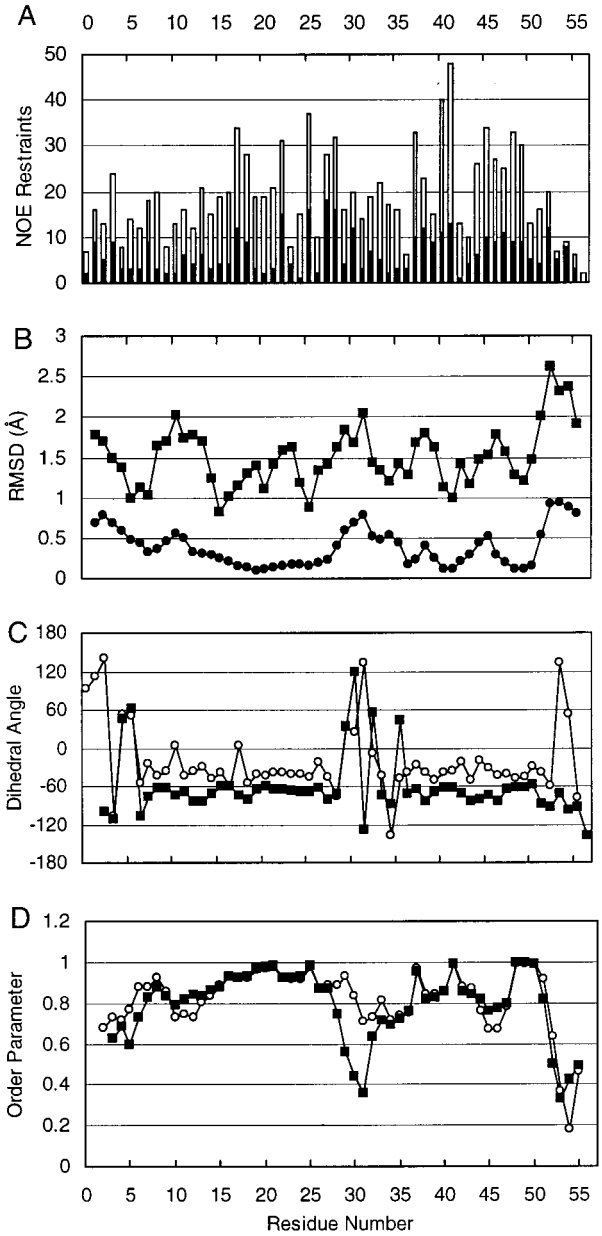

FIGURE 5: Statistics for 18 calculated structures of apoC-I. (A) Distribution of intraresidue (solid columns) and interresidue (open columns) NOE distance restraints used for structure calculation. (B) Average pairwise RMS deviation of backbone atoms (N−C^{α}−C′) (circles) and all heavy atoms (squares). The RMS deviation is smoothed over a three residue window. (C) Average backbone torsion angles ϕ (squares) and ψ (circles). (D) Angular order parameters for the torsion angles shown in panel C. The order parameters are smoothed over a three residue window.

amide resonances, which results in low signal-to-noise ratios for NOE cross-peaks. Figure 7 presents the line widths and the degree of protection from deuterium exchange for backbone amide protons. For the region 12−15 no protection from solvent exchange was observed, and the line widths, in particular for Phe14 and Gly15 (60 and 58 Hz, respectively), are greater than in well-defined helical regions. The H^{α} chemical shift of Phe14 is close to the random coil value (*32*). The chemical shift, line widths, and deuterium exchange data indicate a higher mobility of residues 12−15 relative to ordered helical regions. These experimental results are consistent with the absence of hydrogen bonds to the amide protons of residues 12−15 in the calculated apoC-I structures.

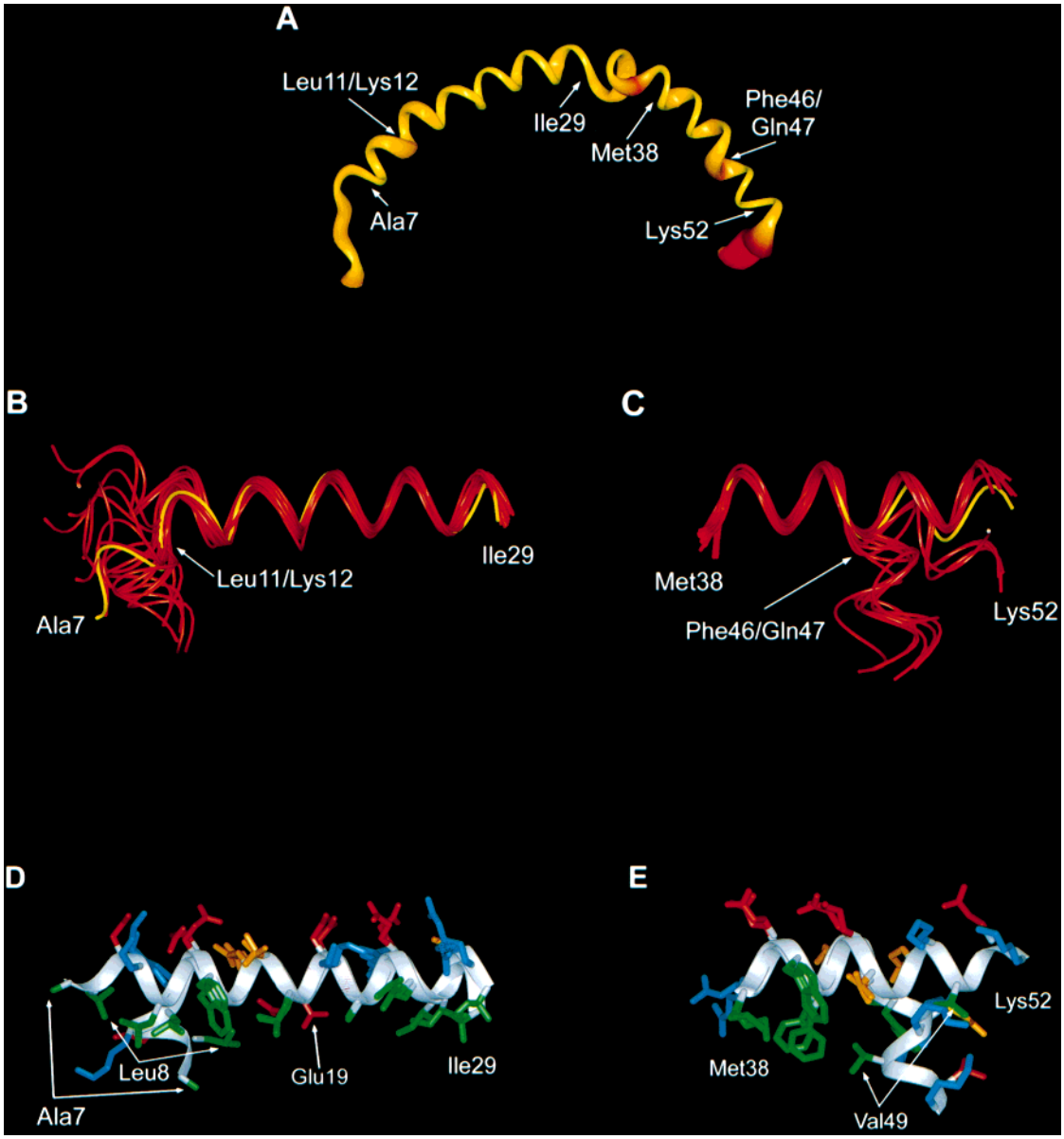

FIGURE 6: Backbone and side chain orientation of the N- and C-terminal helices in apoC-I. (A) Ribbon representation of the structure closest to the mean coordinates of 18 calculated structures. The width and color of the ribbon is modified to reflect the circular variance of the torsion angle ψ. Red shading and greater widths indicate poorly defined regions. The amino acid labels mark the locations of the N- and the C-terminal helices and the positions of highest circular variance within them, which are also the sites of bends. (B and C) Ribbon representations of the N-terminal (B) and C-terminal (C) helices showing the distribution of straight and bent structures. The yellow ribbon represents the structure closest to the mean coordinates of 18 calculated structures (shown in panel A). (D and E) Side-chain orientation in apoC-I comparing straight and bent helical backbones. Shown is the side view of the amphipathic helix with the polar face on top and the nonpolar face on the bottom. The heavy atoms of negatively charged (red), positively charged (blue), and hydrophobic (green) side chains are shown as sticks. The backbone is replaced by a silver ribbon. (D) N-Terminal helix: the molecule is slightly tilted from a side view to show the different position of the Leu8 side chain in straight and bent conformations. In a side view Leu8 would move behind Phe14. The only negatively charged residue intruding into the nonpolar side, Glu19, is also indicated. (E) C-Terminal helix: in a bent conformation Val49 is closer to the aromatic side chains of Trp41 and Phe42.

Bent structures have hydrogen bond distances ($O_i^{C'}-H_{i+4}^{N}$) greater than 2.5 Å and poor O−H−N angles (>35°). The flexibility observed for the region 12−15 in intact apoC-I is also present in the fragment apoC-I(1−38), which was studied previously under similar experimental conditions (*22*). In the apoC-I fragment, increased backbone amide line widths and fast deuterium exchange occurred for the same region, 12−15, and were found to be due to slow conformational exchange. The conformational exchange occurred in the presence of SDS, but not in trifluoroethanol (TFE), suggesting that the effect originated in specific interactions between the peptide and SDS.

A minor distortion of the helical backbone occurs around Leu18, as seen from the torsion angle plot in Figure 5C, and causes a break of the hydrogen bond of Leu18 to Ala22 in 80% of the structures. This result is corroborated by the fast deuterium exchange and broadened amide resonance line widths observed for residues 20−22 (Figure 7). The deviation from helical geometry may be due the intrusion of the Glu19 side chain into the nonpolar face of the amphipathic helix (Figure 6D), which results in unfavorable interactions with SDS.

C-Terminal Lipid-Binding Domain. The C-terminal helix spans the region 38−52, as shown by the average backbone

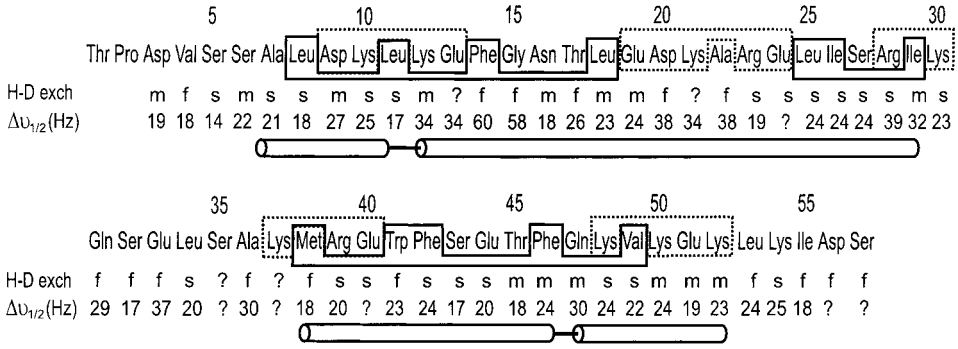

FIGURE 7: Amino acid sequence and sequence specific properties of apoC-I. Hydrophobic clusters and highly charged regions as formed in the calculated structures are boxed with solid and dashed lines, respectively. The approximate exchange rates of backbone amide protons against deuterium, (f = fast, m = medium, s = slow), and the line widths at half peak height, $\Delta\upsilon_{1/2}$ (Hz), of amide protons measured from NOESY cross-peaks are shown below the sequence. Question marks stand for undetermined values due to overlap and low signal-to-noise ratios. The cylinder represents the helical segments with bends indicated by bars.

torsion angles in Figure 5C. The calculated structures for the C-terminal helix are bent at various angles about residues 46/47 (Figure 6C), which is associated with relatively increased RMS deviations (Figure 5B), lower angular order parameters (Figure 5D), and the break of the hydrogen bond between Ser43 and Gln47. Experimental support for a bend in the C-terminal helix comes from the slightly increased line widths and the deuterium exchange of the Gln47 amide proton, which is faster than the otherwise slow exchange observed in the C-terminal helix (Figure 7). The C-terminal helix in intact apoC-I may be compared to the fragment apoC-I(35−53), which was found to adopt a linear helix formed by residues 39−51 (*21*). While the region 39−51 shows no differences larger than 0.1 ppm in H^{α} chemical shifts, the helical Ser43 H^{α}-Phe46 H^{N} NOE cross-peak in intact apoC-I is weaker than in apoC-I(35−53). A number of NOE contacts are observed between the side chains of Met38 and Trp41/Phe42 in intact apoC-I, which are absent in the smaller fragment and suggest a tighter packing of hydrophobic side chains in the intact apolipoprotein. These data are also in favor of a slightly bent C-terminal helix in intact apoC-I.

Other Regions. The interhelical region in apoC-I includes residues 30−37. This region is poorly defined as shown by high backbone RMS deviations (Figure 5B) and low angular order parameters (Figure 5D). The average backbone dihedral angles of most residues in the region 30−37 are outside the allowed areas of the Ramachandran plot (Figure 5C). Careful examination of the NOESY spectra shows that NOE cross-peaks for residues 30−37 are not hidden or ambiguous due to resonance overlap (Figure 3). The absence of NOE restraints is probably the result of higher backbone mobility. The H^{α} chemical shifts of residues 31−33, which are close to the random coil values (*32*), and the fast deuterium exchange of backbone amide protons (Figure 7) further corroborate an unordered structure in the region 30−37.

The six N-terminal residues lack a well-defined structure, although helical propensity is indicated by H^{α} secondary shifts starting with residue 4 (*32*). We attribute this deviation to an insufficient number of distance restraints being available for structure calculations due to NOE cross-peak overlap (Figure 3). The five C-terminal residues are unstructured, which is consistent with H^{α} chemical shifts close to random coil values and fast deuterium exchange of backbone amide protons (Figure 7).

DISCUSSSION

In the present study, we have determined the structure of apoC-I in complexes with SDS. As shown by CD data, addition of SDS to apoC-I causes the protein to adopt a helical content similar to that found with phosholipids. The apoC-I helicity estimated by CD analysis (54%) is lower than that calculated from the amount of residues in helical regions, 7−29 and 38−52, of the NMR structure (67%). The discrepancy between these values may be due to the bends found in both helices, which represent deviations from ideal geometry. The helical content of the NMR derived apoC-I conformation drops to 61%, if only well-defined helical regions are included. Also, the exchange between SDS-bound and unbound apoC-I molecules, associated with an unfolding of the helices, may contribute to the lower helicity observable by CD spectroscopy (*41*, *42*).

The calculated ensemble of structures for apoC-I shows that the protein forms two amphipathic helices, 7−29 and 38−52, separated by an unordered region 30−37. The structure of apoC-I bound to SDS is consistent with results from previous studies on apoC-I and its fragments using phospholipid vesicles. First, the lipid binding amphipathic helices of apoC-I were predicted from primary sequence analysis to be located in the regions 7−32 and 33−54; the break between the two helices was predicted due to a break in the periodicity of hydrophobic and hydrophilic amino acids required to form a amphipathic helix (*18*). Second, the apoC-I fragment 1−38 was found to strongly bind to phospholipid vesicles and form a helical structure (*43*), which is consistent with the N-terminal helix found in apoC-I when bound to SDS. Phospholipid-binding studies with apoC-I(32−57) have shown that this fragment binds, accompanied by helix formation, to DMPC vesicles at a peptide-to-lipid ratio of 1:30 (*44*), in agreement with the presence of a C-terminal helix in intact apoC-I when bound to SDS.

Both helices in apoC-I contain poorly defined regions, resulting in a distribution of more or less bent helices (Figure 6, panels B and C). In evaluating the results of the structure calculation, we note that an exchange between bent and straight backbone conformations in the N-terminal helix is consistent with the H^{α} secondary shifts, deuterium exchange data and backbone amide line widths (Figures 3 and 7). For the C-terminal helix, mostly slow deuterium exchange, fairly uniform backbone amide line widths and a significant effect

of aromatic ring currents on the chemical shifts of residues 45−50 indicate that the C-terminal helix is less flexible and probably more tightly lipid bound than the N-terminal helix. The large variation of the bend in the calculated structures for the C-terminal helix may be explained by the absence of NOE restraints due to cross-peak overlap in the NOESY spectra of apoC-I. Since an exchange between strongly bent and straight backbone conformations in the C-terminal helix is not conclusive from all the available experimental data, we suggest that the C-terminal helix assumes the average conformation, e.g., slightly bent, of those in the calculated structural ensemble shown in Figure 6C.

The unstructured and flexible interhelical region permits an independent arrangement of the two helices in the calculated apoC-I structures, including parallel helices. While the angle spanned by the N- and C-terminal helices may fluctuate over a wide region, a stable parallel alignment of both helices is not found in the presence of SDS, since we did not observe NOE contacts between the N-terminal and the C-terminal helix. However, this fold may be present in solution in the absence of lipid. Monomeric intact apoC-I is 30% helical in aqueous solution (*34*) while the fragments, 1−38 and 35−53, are unstructured (*21*, *22*). This difference might be related to structural stabilization by helix−helix interactions in intact apoC-I. Indeed, preliminary analysis of apoC-I by X-ray crystallography indicates a helix bundle structure formed by two apoC-I molecules (*45*) which, in our view, is the most probable solution structure.

Role of Hydrophobic Residues. Hydrophobic interactions between nonpolar residues of the amphipathic protein and the fatty acyl chains of the lipid are thought to be the major factor in lipoprotein stabilization (*17*). Figure 7 shows the apoC-I sequence pointing out closely spaced charged residues and closely spaced hydrophobic residues. The hydrophobic side chains form three clusters, which are (1) Leu8, Leu11, Phe14, and Leu18, (2) Leu25, Ile26, and Ile29 in the N-terminal helix, and (3) Met38, Trp41, Phe42, Phe46, and Val49 in the C-terminal helix. In the N-terminal helix, the bend at Leu11/Lys12 decreases the average distance between the hydrophobic residues Leu8 on one side and Phe14 and Leu18 on the other side (Figure 6D) by 2−3 Å, respectively, thus increasing the density of the hydrophobic cluster Leu8, Leu11, Phe14, and Leu18. Similarly, in a bent C-terminal helix, the residue Val49 moves, on average, 2−3 Å closer to the hydrophobic residues Met38, Trp41, and Phe42 (Figure 6E). The tendency of hydrophobic residues to cluster with a concomitant bend in the amphipathic helix has also been observed for the apoE fragment 263−286 (*46*). The formation of hydrophobic clusters by apolipoprotein helices may result in a helical motif that enhances binding to curved lipid surfaces, such as those of small HDL particles.

As outlined above, the C-terminal helix appears to be less flexible and may be more tightly lipid bound than the N-terminal helix, although it contains only one hydrophobic cluster, while the N-terminal helix contains two. Part of the C-terminal hydrophobic cluster is a well-defined arrangement of the closely spaced side chains of Met38, Trp41, and Phe42. The Trp41 and Phe42 side chains form an aromatic pair, which has been shown to stabilize protein structure by 1−2 kcal/mol (*47*). In the calculated structures, both aromatic rings are oriented perpendicular to one another and Trp41 H4 and H5 are, on average, 4 Å away from the center of the Phe42 ring. The orientation of the Met38 side chain suggests that the sulfur atom may also interact with the Trp41 and Phe42 aromatic rings (*48*). When viewed down the $C^{\gamma}-S$ bond, the $S-C^{\epsilon}$ bond assumes a gauche orientation with respect to the $C^{\beta}-C^{\gamma}$ bond in 72% of the calculated structures and the ϵ-methyl group is pointed toward both aromatic rings. The average distance of the sulfur atom to both aromatic rings is 6 Å. In addition to aromatic−aromatic and hydrophobic interactions, the sulfur−aromatic interactions may enhance the stability of the triad Met38, Trp41, and Phe42. From the above data, the different mobility, observed for the N- and C-terminal helices in apoC-I, appears to be a function of side-chain composition rather than length of the amphipathic helix. We agree with Wang et al. (*46*) who proposed that aromatic residues play a dominant role in anchoring apolipoproteins to lipid surfaces. Strong lipid-binding domains near the C-terminus of apolipoproteins have also been demonstrated for apoE (*49*) and apoA-I (*50*) and have been proposed to control the rapid capture and release of apolipoproteins during transfer between the lipoprotein particles in circulation (*46*).

The flexibility in the long N-terminal helix may be an asset in binding to lipoprotein particles of different size and curvature, such as VLDL (25−70 nm) and HDL (4−10 nm) (*51*), which are the major pools of apoC-I in blood plasma. Monoclonal antibodies raised against apoC-I were specific for an amino-terminal epitope, located between residues 1−38 (*52*). One possible explanation for the antigenicity of lipid-binding domains in apolipoproteins is their conformational flexibility (*53*). Taken together, these results are consistent with our conclusion that the N-terminal helix in apoC-I is more flexible than the C-terminal helix. Antibodies raised against VLDL-bound apoC-I competed more effectively with apoC-I on native VLDL than on native HDL (*47*), which suggests that the conformation of the N-terminal helix is slightly different in VLDL and HDL. Therefore, the N-terminal helix may adapt to lipoprotein size and composition.

Role of Charged Residues. The function of charged residues in amphipathic helices is not well understood. In class A amphipathic helices, lysine and arginine residues are thought to increase the lipid affinity by means of hydrophobic interaction between their alkyl chains and the lipid acyl chains. Charged groups may add stability to the protein lipid complex by forming weak ionic interactions with the phospholipid headgroups or stabilize the helix by intrahelical ion pairs (*17*). The positively charged residues in apoC-I are located at the polar/nonpolar interface of the amphipathic helix while negatively charged residues, with the exception of Glu19, form a line at the center of the polar face (Figure 6, panels D and E). Ion pairs between oppositely charged side chains three or four residues apart are proposed to stabilize the helical structure by 0.5−5 kcal/mol; lower values prevail for solvent exposed ion pairs (*54*, *55*). The apoC-I sequence has seven potential ion pairs in the helical regions (Figure 7). In the calculated structures, the average distances between charged groups in these pairs are 6.5−9.5 Å. Hence, the helical structure of apoC-I in the presence of SDS is not stabilized by intrahelical ion pairs. Similar conclusions were drawn for the smaller fragments of apoC-I (*21*, *22*). Further evidence for the absence of ion pairs is given by the pK_as of acidic side chains in apoC-I(1−38), which are equal to or

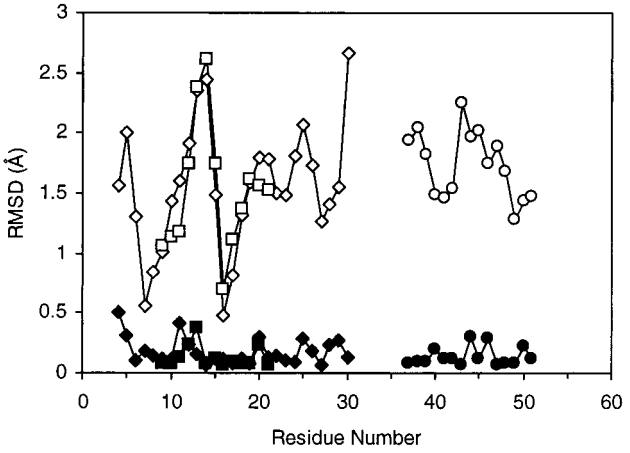

FIGURE 8: Pairwise RMS deviation of three apoC-I fragments against intact apoC-I. The RMS deviation is computed for the well-defined regions of either peptide and is smoothed over a three residue window. Diamonds: apoC-I(1−38), residues 4−30, against apoC-I. Squares: apoC-I(7−24), residues 9−21, against apoC-I. Circles: apoC-I(35−53), residues 37−51, against apoC-I. Open signs indicate the RMS deviation for all heavy atoms and filled signs indicate the RMS deviation for backbone atoms ($N-C^{\alpha}-C'$).

above the solution pK_as (ion pairs would be indicated by lower pK_as) (*22*).

The apoC-I sequence contains regions of closely spaced charged residues, which alternate with regions of nonpolar and uncharged, polar residues (Figure 7). The regions of high charge density, Asp9-Glu13 and Glu19-Arg23, correlate with the bend observed at residues 11/12 and the distortion around Glu19 and possibly contribute to the flexibility observed in the N-terminal helix by decreasing the hydrophobicity in these areas. In this respect, it is interesting to note that the interfacial Glu19 in apoC-I is at the 13th position in a 22 residue long helix, 7−29, comprising the first two 11mer amino acid repeats. The placement of a glutamic acid residue at the 13th position near the nonpolar face of the amphipathic helix of apoA-I peptide analogues resulted in a markedly reduced lipid affinity combined with an increased LCAT activating ability (*56*).

Comparison of apoC-I and Its Fragments. Previously, we have determined the structures of three apoC-I peptides under similar experimental conditions (*21*, *22*). The conformations of apoC-I and its peptides may be compared to determine how well the structure of the intact protein is represented by its fragments. In Figure 8, the atomic RMS deviation of each fragment is plotted against intact apoC-I. The average local RMS deviations are 0.13 ± 0.09 Å for apoC-I(7−24), 0.13 ± 0.08 Å for apoC-I(35−53), and 0.18 ± 0.11 Å for apoC-I(1−38), indicating that the local structure of each apoC-I fragment agrees well with intact apoC-I. The RMS deviation for the N-terminal helix is higher for residues 11 [apoC-I(1−38)] and 13 [apoC-I(7−24)], which reflects the flexibility found in the region 12−15 of apoC-I. The most remarkable structural difference occurs between apoC-I(7−24) and intact apoC-I. For apoC-I(7−24), all structures of the calculated ensemble form straight helices while intact apoC-I is bent at residues 11/12. In the fragment 7−24, the residue Leu8 is part of the fraying peptide terminus and may not interact strongly with lipid. However, in intact apoC-I, the residue Leu8 is part of a helical turn and participates in the hydrophobic cluster Leu8, Leu11, Phe14, and Leu18. Apparently, in the fragment apoC-I(7−24), this lipid-binding site is truncated and is too short to simulate the intact apoC-I structure. The longer fragment apoC-I(1−38) shows the same structural features as intact apoC-I, since it comprises the complete N-terminal lipid-associating domain.

Implications for apoC-I Structure−Function Relationship. ApoC-I is a model for the primary LCAT activator apoA-I. Depending on the lipid substrate, apoC-I activates LCAT 10−45% relative to apoA-I (*2*, *57*, *58*). It has been shown by several studies that the central amphipathic helical domains in apoA-I play a critical role in LCAT activation (*50*, *59*, *60*). It is interesting to note that these central helices in apoA-I have lower lipid affinities than the terminal helices (*61*). Our NMR studies of apoC-I suggest that the N-terminal helix is more mobile and has a lower lipid affinity than the C-terminal helix. The apoC-I fragment 1−38, containing the N-terminal lipid-binding domain, does not activate LCAT (*1*). The apoC-I fragments 32−57 and 24−57, containing the C-terminal lipid-binding domain, activate LCAT to a minor extent; however, the fragment 17−57 contains all structural requirements for LCAT activation by apoC-I (*44*). In light of the structure presented in this report, the above results suggest that activation of LCAT by apoC-I requires the tightly lipid-bound C-terminal helix *and* the less tightly lipid-bound N-terminal helix connected by a flexible hinge. We hypothesize that the C-terminal helix anchors apoC-I to the lipoprotein surface, while the flexible hinge would allow the N-terminal helix to lift off the lipoprotein surface and make contact with the enzyme. Moreover, these two types of helices may be the necessary structural building blocks for LCAT activation by apolipoproteins in general.

ACKNOWLEDGMENT

We thank R. Storjohann and J. C. Cramer for fruitful discussions. We also thank Dr. M. Okon for help in implementing the heteronuclear pulse sequences.

REFERENCES

1. Soutar, A. K., Garner, C. W., Baker, H. N., Sparrow, J. T., Jackson, R. L., Gotto, A. M., and Smith, L. C. (1975) *Biochemistry 14*, 3057−64.
2. Jonas, A., Sweeny, S. A., and Herbert, P. N. (1984) *J. Biol. Chem. 259*, 6369−75.
3. Glomset, J. A. (1968) *J. Lipid Res. 9*, 155−67.
4. Poensgen, J. (1990) *Biochim. Biophys. Acta 1042*, 188−92.
5. Kinnunen, P. K., and Ehnolm, C. (1976) *FEBS Lett. 65*, 354−7.
6. Tournier, J. F., Bayard, F., and Tauber, J. P. (1984) *Biochim. Biophys. Acta 804*, 216−20.
7. Weisgraber, K. H., Mahley, R. W., Kowal, R. C., Herz, J., Goldstein, J. L., and Brown, M. S. (1990) *J. Biol. Chem. 265*, 22453−9.
8. Sehayek, E., and Eisenberg, S. (1991) *J. Biol. Chem. 266*, 18259−67.
9. Jong, M. C., Gijbels, M. J., Dahlmans, V. E., Gorp, P. J., Koopman, S. J., Ponec, M., Hofker, M. H., and Havekes, L. M. (1998) *J. Clin. Invest. 101*, 145−52.
10. McLachlan, A. D. (1977) *Nature 267*, 465−6.
11. Luo, C. C., Li, W. H., Moore, M. N., and Chan, L. (1986) *J. Mol. Biol. 187*, 325−40.
12. Jackson, R. L., Sparrow, J. T., Baker, H. N., Morrisett, J. D., Taunton, O. D., and Gotto, A. M., Jr. (1974) *J. Biol. Chem. 249*, 5308−13.
13. Shulman, R. S., Herbert, P. N., Wehrly, K., and Fredrickson, D. S. (1975) *J. Biol. Chem. 250*, 182−90.

14. Davison, P. J., Norton, P., Wallis, S. C., Gill, L., Cook, M., Williamson, R., and Humphries, S. E. (1986) *Biochem. Biophys. Res. Commun. 136*, 876−84.
15. Lauer, S. J., Walker, D., Elshourbagy, N. A., Reardon, C. A., Levy-Wilson, B., and Taylor, J. M. (1988) *J. Biol. Chem. 263*, 7277−86.
16. Poduslo, S. E., Neal, M., and Schwankhaus, J. (1995) *Neurosci. Lett. 201*, 81−3.
17. Segrest, J. P., Jackson, R. L., Morrisett, J. D., and Gotto, A. M., Jr. (1974) *FEBS Lett. 38*, 247−58.
18. Segrest, J. P., Jones, M. K., De Loof, H., Brouillette, C. G., Venkatachalapathi, Y. V., and Anantharamaiah, G. M. (1992) *J. Lipid Res. 33*, 141−66.
19. McDonnell, P. A., and Opella, S. J. (1993) *J. Magn. Res., Ser. B 102*, 120−25.
20. Henry, G. D., and Sykes, B. D. (1994) *Methods Enzymol. 239*, 515−35.
21. Rozek, A., Buchko, G. W., and Cushley, R. J. (1995) *Biochemistry 34*, 7401−8.
22. Rozek, A., Buchko, G. W., Kanda, P., and Cushley, R. J. (1997) *Protein Sci. 6*, 1858−68.
23. Perczel, A., Park, K., and Fasman, G. D. (1992) *Anal. Biochem. 203*, 83−93.
24. Greenfield, N., and Fasman, G. D. (1969) *Biochemistry 8*, 4108−16.
25. Braunschweiler, L., and Ernst, R. R. (1983) *J. Magn. Res. 53*, 521−28.
26. Rance, M., Sorensen, O. W., Bodenhausen, G., Wagner, G., Ernst, R. R., and Wuthrich, K. (1983) *Biochem. Biophys. Res. Commun. 117*, 479−485.
27. Jeener, J., Meier, B. H., Bachmann, P., and Ernst, R. R. (1979) *J. Chem. Phys. 71*, 4546−4553.
28. Otting, G., Senn, H., Wagner, G., and Wuthrich, K. (1986) *J. Magn. Res. 70*, 500−5.
29. Fesik, S. W., Gampe, R. T., and Rockway, T. W. (1987) *J. Magn. Res. 74*, 366−71.
30. Bodenhausen, G., and Ruben, D. J. (1980) *Chem. Phys. Lett. 69*, 185−9.
31. Marion, D., Driscoll, P. C., Kay, L. E., Wingfield, P. T., Bax, A., Gronenborn, A. M., and Clore, G. M. (1989) *Biochemistry 28*, 6150−6.
32. Rozek, A., Sparrow, J. T., Weisgraber, K. H., and Cushley, R. J. (1998) *Biochem. Cell Biol. 76*, 267−75.
33. Dauber-Osguthorpe, P., Roberts, V. A., Osguthorpe, D. J., Wolff, J., Genest, M., and Hagler, A. T. (1988) *Proteins 4*, 31−47.
34. Gursky, O., and Atkinson, D. (1998) *Biochemistry 37*, 1283−91.
35. Osborne, J. C., Jr., Bronzert, T. J., and Brewer, H. B., Jr. (1977) *J. Biol. Chem. 252*, 5756−60.
36. Swaney, J. B., and Weisgraber, K. H. (1994) *J. Lipid Res. 35*, 134−42.
37. Wishart, D. S., Sykes, B. D., and Richards, F. M. (1992) *Biochemistry 31*, 1647−51.
38. Kabsch, W., and Sander, C. (1983) *Biopolymers 22*, 2577−637.
39. Hyberts, S. G., Goldberg, M. S., Havel, T. F., and Wagner, G. (1992) *Protein. Sci. 1*, 736−51.
40. Segrest, J. P., De Loof, H., Dohlman, J. G., Brouillette, C. G., and Anantharamaiah, G. M. (1990) *Proteins 8*, 103−17.
41. Hirst, J. D., and Brooks, C. L., III (1994) *J. Mol. Biol. 243*, 173−8.
42. Hennessey, J. P., Jr., and Johnson, W. C., Jr. (1982) *Anal. Biochem. 125*, 177−88.
43. Jackson, R. L., Morrisett, J. D., Sparrow, J. T., Segrest, J. P., Pownall, H. J., Smith, L. C., Hoff, H. F., and Gotto, A. M., Jr. (1974) *J. Biol. Chem. 249*, 5314−20.
44. Soutar, A. K., Sigler, G. F., Smith, L. C., Gotto, A. M., Jr., and Sparrow, J. T. (1978) *Scand. J. Clin. Lab. Invest. Suppl. 150*, 53−8.
45. Weisgraber, K. H., Newhouse, Y. M., and McPherson, A. (1994) *J. Mol. Biol. 236*, 382−4.
46. Wang, G., Pierens, G. K., Treleaven, W. D., Sparrow, J. T., and Cushley, R. J. (1996) *Biochemistry 35*, 10358−66.
47. Burley, S. K., and Petsko, G. A. (1985) *Science 229*, 23−8.
48. Reid, K. S. C., Lindley, P. F., and Thornton, J. M. (1985) *FEBS Lett. 190*, 209−13.
49. Sparrow, J. T., Sparrow, D. A., Fernando, G., Culwell, A. R., Kovar, M., and Gotto, A. M., Jr. (1992) *Biochemistry 31*, 1065−8.
50. Holvoet, P., Zhao, Z., Vanloo, B., Vos, R., Deridder, E., Dhoest, A., Taveirne, J., Brouwers, E., Demarsin, E., and Engelborghs, Y., et al. (1995) *Biochemistry 34*, 13334−42.
51. Scanu, A. M., Edelstein, C., and Shen, B. W. (1982) *Lipid−Protein Interactions in Plasma Lipoproteins. Model: High-Density Lipoproteins*, Vol. 1, John Wiley & Sons, New York.
52. Krul, E. S., Oida, K., and Schonfeld, G. (1987) *J. Lipid Res. 28*, 818−27.
53. Marcel, Y. L., Provost, P. R., Koa, H., Raffai, E., Dac, N. V., Fruchart, J. C., and Rassart, E. (1991) *J. Biol. Chem. 266*, 3644−53.
54. Merutka, G., and Stellwagen, E. (1991) *Biochemistry 30*, 1591−4.
55. Smith, J. S., and Scholtz, J. M. (1998) *Biochemistry 37*, 33−40.
56. Anantharamaiah, G. M., Venkatachalapathi, Y. V., Brouillette, C. G., and Segrest, J. P. (1990) *Arteriosclerosis 10*, 95−105.
57. Albers, J. J. (1978) *Scand. J. Clin. Lab. Invest. Suppl. 150*, 48−52.
58. Steyrer, E., and Kostner, G. M. (1988) *Biochim. Biophys. Acta 958*, 484−91.
59. Minnich, A., Collet, X., Roghani, A., Cladaras, C., Hamilton, R. L., Fielding, C. J., and Zannis, V. I. (1992) *J. Biol. Chem. 267*, 16553−60.
60. Sorci-Thomas, M. G., Curtiss, L., Parks, J. S., Thomas, M. J., and Kearns, M. W. (1997) *J. Biol. Chem. 272*, 7278−84.
61. Palgunachari, M. N., Mishra, V. K., Lund-Katz, S., Phillips, M. C., Adeyeye, S. O., Alluri, S., Anantharamaiah, G. M., and Segrest, J. P. (1996) *Arterioscler. Thromb. Vasc. Biol. 16*, 328−38.

BI982966H